frontiers in Physics

ORIGINAL RESEARCH
published: 15 June 2021
doi: 10.3389/fphy.2021.691034

Optical Response of Sila-Fulleranes in Interaction With Glycoproteins for Environmental Monitoring

Mohammad Qasemnazhand[1], *Farhad Khoeini*[1]* *and Farah Marsusi*[2]

[1]Department of Physics, University of Zanjan, Zanjan, Iran, [2]Department of Physics and Energy Engineering, Amirkabir University of Technology, Tehran, Iran

In this paper, we introduce new features of silicon in fullerane structures. Silicon, when placed in a fullerane structure, increases its electron affinity and electrophilicity index, compared to placement in a diamondoids structure. These nanoparticles can be used to make optical sensors to detect viral environments. In this work, we theoretically examine the changes in the UV-Visible spectrum of sila-fulleranes by interacting with viral spikes. As a result, we find out how the color of silicon nanoparticles changes when they interact with viruses. We apply N- and O-Links for viral glycoprotein structures, and $Si_{20}H_{20}$ silicon dodecahedrane, respectively. Our computational method to obtain optimal structures and their energy in the ground and excited states, is density functional theory (DFT). Besides, to get the UV-Visible spectrum, time-dependent density functional theory (TD-DFT) approach has been used. Our results show that the color of sila-dodecahedrane is white, and turns green in the face of viral spikes. We can use the optical sensitivity of silicon nanoparticles, especially to identify environments infected with the novel coronavirus.

Keywords: sila-fullerane, electrophilicity index, density functional theory, novel coronavirus, glycoproteins

OPEN ACCESS

Edited by:
Ambrish Kumar Srivastava,
Deen Dayal Upadhyay Gorakhpur University, India

Reviewed by:
Ruby Srivastava,
Centre for Cellular and Molecular Biology (CCMB), India
Abhishek Kumar,
University of Lucknow, India

***Correspondence:**
Farhad Khoeini
khoeini@znu.ac.ir

Specialty section:
This article was submitted to Physical Chemistry and Chemical Physics, a section of the journal Frontiers in Physics

Received: *05 April 2021*
Accepted: *31 May 2021*
Published: *15 June 2021*

Citation:
Qasemnazhand M, Khoeini F and Marsusi F (2021) Optical Response of Sila-Fulleranes in Interaction With Glycoproteins for Environmental Monitoring. Front. Phys. 9:691034. doi: 10.3389/fphy.2021.691034

INTRODUCTION

If environmental health can reduce the role of viruses, the complex issue of treating viral patients will be removed from its critical state. But with the spread of human societies, can old methods clean the environment from microbial contamination? These methods are based on disinfecting suspicious, susceptible, and busy places. These are very costly due to the large statistical target population; as a result, it is sometimes impossible to do so [1]. Therefore, the need for substances that detect microbial contamination of the environment, whether viral or bacterial, etc., is felt more and more.

Nanoparticles can be sensitive to the viral environment. This sensitivity can appear as changes in color, light or even electrical properties. Metal nanoparticles have previously been studied to identify a variety of microbes. However, they usually have high chemical softness, which not only causes them to be unstable, but also causes unpredictable changes in biological systems [2, 3]. From non-metallic nanoparticles, carbon can be affected by the environment, if it is located in a structure with sp^2 orbital hybridization, such as graphene, fullerenes, etc., due to the resonance of unlocated electrons, and so can be used as a sensor [4–7]. But graphene-based nanoparticles also always tend to oxidize [8].

Silicon, as the most popular metalloid, exhibits significant properties when placed in the form of nanoparticles. In 2013, Moore et al. showed that silicon nanoparticles can be used as optical sensors [9]. Biocompatibility and sensitivity to surface factors make silicon nanoparticles more attractive to therapeutic agents in biological systems [10–12]. In this study, we investigate the sensitivity of silicon nanoparticles to biological contamination, and introduce a type of nanoparticles as a virus-sensitive

identifier [13–16]. We indicate that when silicon is placed in a fullerane structure, its electron sensitivity increases, so that we do our study on sila-fulleranes [17–21]. Since the electronic properties of sila-fulleranes with sizes between 1 and 2 nm, are very close to each other, we focus on our smallest samples to save on computational costs [22]. Also, to remove the edge factors, we have selected the most symmetric sila-fullerane for this purpose [23–25]. As a result, we select the sila-dodecahedrane with the chemical formula $Si_{20}H_{20}$, which has icosahedral (Ih) symmetry [26, 27]. Finally, we generalize the results to a set of sila-fulleranes.

COMPUTATIONAL METHOD

Our calculations are based on density functional theory. We obtain the optimal and stable geometry of the structures and their energy in the ground and excited states, by B3LYP hybrid functional [28–30]. Using time-dependent density functional theory, we obtained the UV-visible spectrum for the studied structures [31, 32]. We describe the orbitals of the atoms by basis set, which include the split valence, polarized and diffuse functions, that is 6-31 + G (d,p) basis set [33, 34, 35]. The calculations are performed by the Gaussian package [36, 37]. We also used AIM2000 software to analyze the interaction between the structure of the sensor and the glycoproteins studied [38].

RESULTS

Virus spikes are usually made up of glycoproteins. Glycoprotein is a combination of protein and carbohydrate. There are different types of glycoproteins, however, the most common glycoproteins that make virus spikes, like the spike of the coronaviruses, are O-Link and N-Link types [39–43]. If the causative of carbohydrate-binding to protein is oxygen atoms, it is called O-Link, and if it is nitrogen atoms, it is called N-Link. The structure of these two types of glycoproteins is shown in **Figure 1**.

In this study, we propose that silicon nanoparticles have the ability to sense N-Link and O-Link glycoproteins. Because, in addition to biocompatibility, they are also electron sensitive. Although silicon is usually placed in the diamond structure, but when silicon placed in a fullerane structure, the rate of quantum confinement effect will be smaller. Unlike sila-diamondoids, sila-fulleranes does not consist of pure sp^3 hybridization structure. Especially if fulleranes structures consist of a number of fused hexagon rings (NFHR), deviation from sp^3 hybridization occurs more frequently [22]. Finally, this deviation causes difference in the electronic properties of sila-fullerans and sila-diamondoids.

Using the following equations [44–47], we can obtain electronic information, such as the HOMO-LUMO gap, chemical potential, chemical hardness, and finally an estimate of electron affinity:

$$E_{Gap} = E_{LUMO} - E_{HOMO}. \quad (1)$$

$$\mu = \frac{(E_{HOMO} + E_{LUMO})}{2}. \quad (2)$$

TABLE 1 | A list of some of the electronic features of the first six structures of Sila-fullerane (in unit eV).

Nanoparticle	HOMO	LUMO	E_{Gap}	μ	η	EA	IP	ω
$Si_{20}H_{20}$	−6.83	−2.36	4.48	−4.60	2.24	2.36	6.83	4.72
$Si_{24}H_{24}$	−6.70	−2.39	4.31	−4.54	2.16	2.39	6.70	4.78
$Si_{28}H_{28}$	−6.88	−2.49	4.39	−4.69	2.20	2.49	6.88	5.00
$Si_{30}H_{30}$	−6.86	−2.48	4.39	−4.67	2.20	2.48	6.86	4.97
$Si_{36}H_{36}$	−6.78	−2.49	4.29	−4.64	2.14	2.49	6.78	5.02
$Si_{60}H_{60}$	−7.05	−2.59	4.46	−4.82	2.23	2.59	7.05	5.20

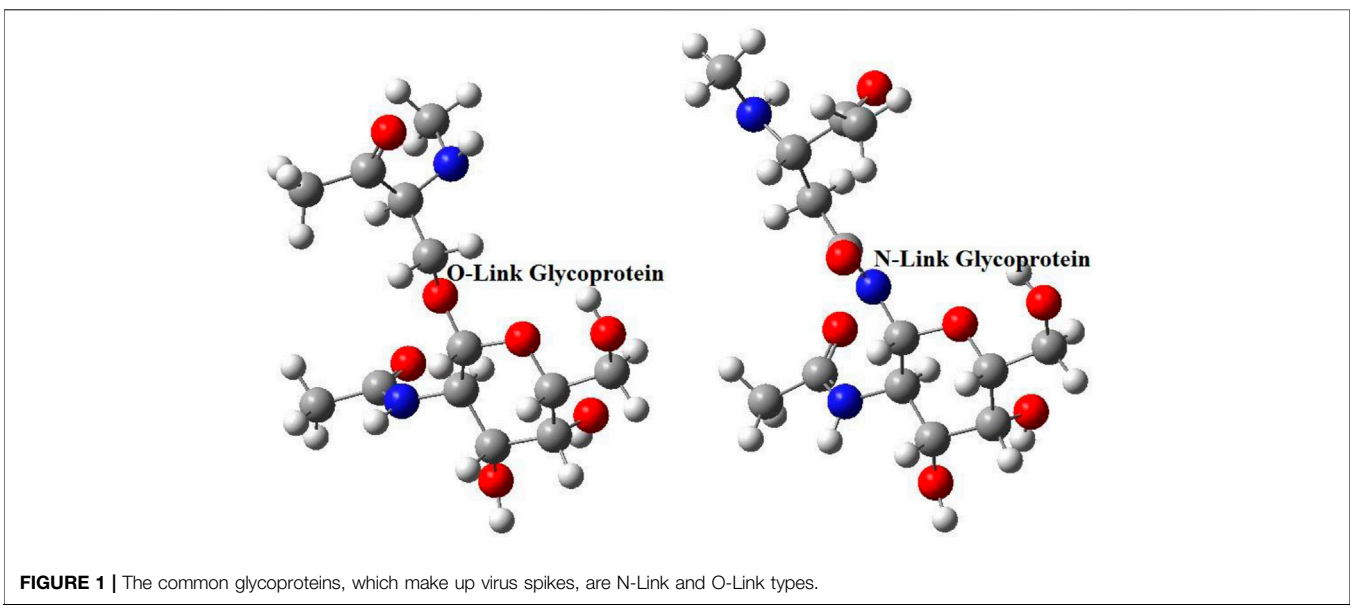

FIGURE 1 | The common glycoproteins, which make up virus spikes, are N-Link and O-Link types.

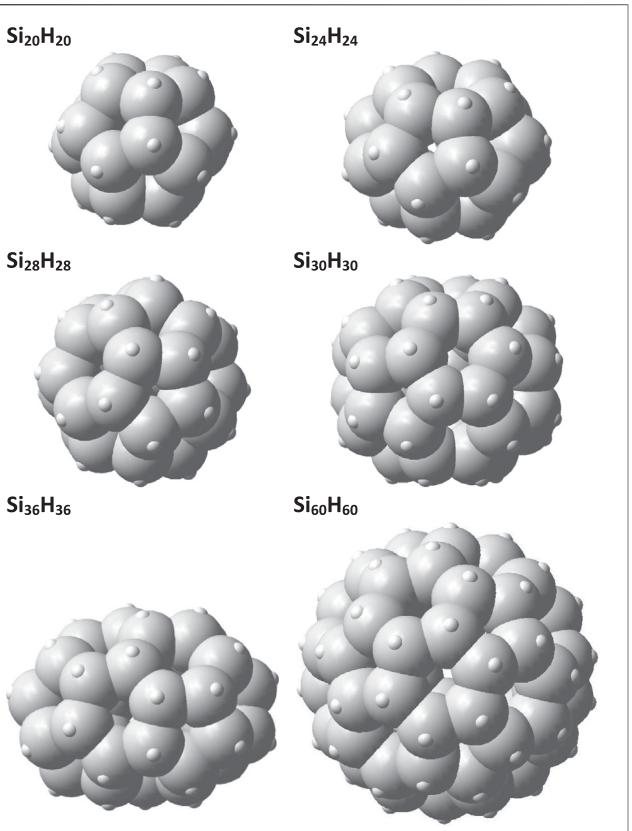

FIGURE 2 | The first six structures of Sila-fulleranes.

$$\eta = \frac{(E_{HOMO} - E_{LUMO})}{2}. \tag{3}$$

$$EA = -E_{LUMO}. \tag{4}$$

$$IP = -E_{HOMO}. \tag{5}$$

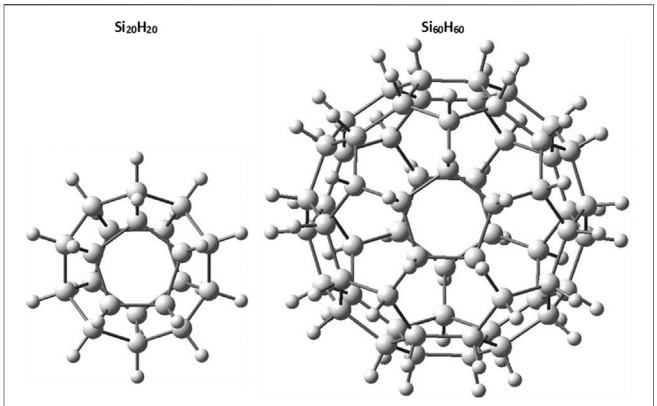

FIGURE 4 | $Si_{20}H_{20}$ and $Si_{60}H_{60}$ structures, which have icosahedral symmetry.

The new index, electrophilicity, can be obtained using chemical potential and chemical hardness through **Eq. 6**. Regarding electrophilicity, the difference between the type of structures is clearly visible [48, 49].

$$\omega = \frac{\mu^2}{2\eta}. \tag{6}$$

We calculated the above electronic information for the six structures of sila-fulleranes. You can see the electronic information of them in **Table 1**.

Our previous researches on silicon nanoparticles shows that diagram of quantum confinement effect (QCE) for sila-fulleranes smoothly change than sila-diamondoids, especially in the range of 1–2 nm [22]. As a result, the HOMO-LUMO gap of fulleranes close to each other in this range, and because many properties such as chemical hardness, chemical potential and indexes such as electrophilicity are derived from this gap, so the properties of

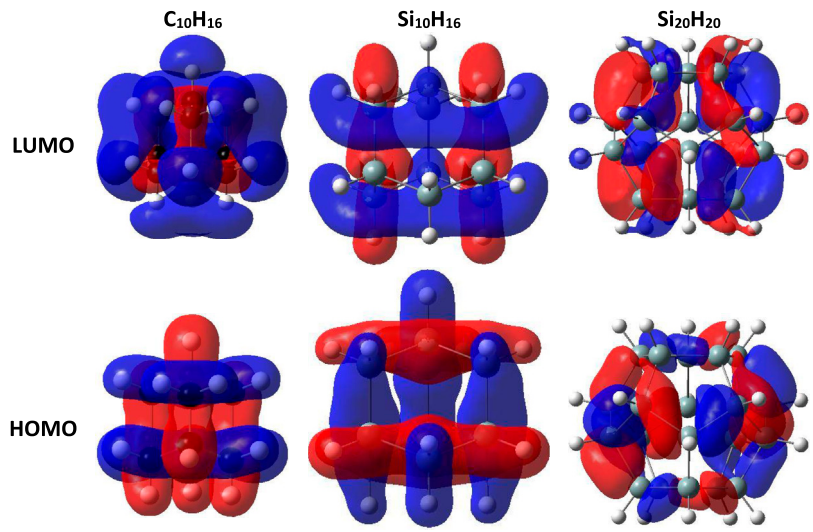

FIGURE 3 | The HOMO and LUMO orbitals for diamondoids, sila-diamondoids and sila-fulleranes (Isovalue = 0.02).

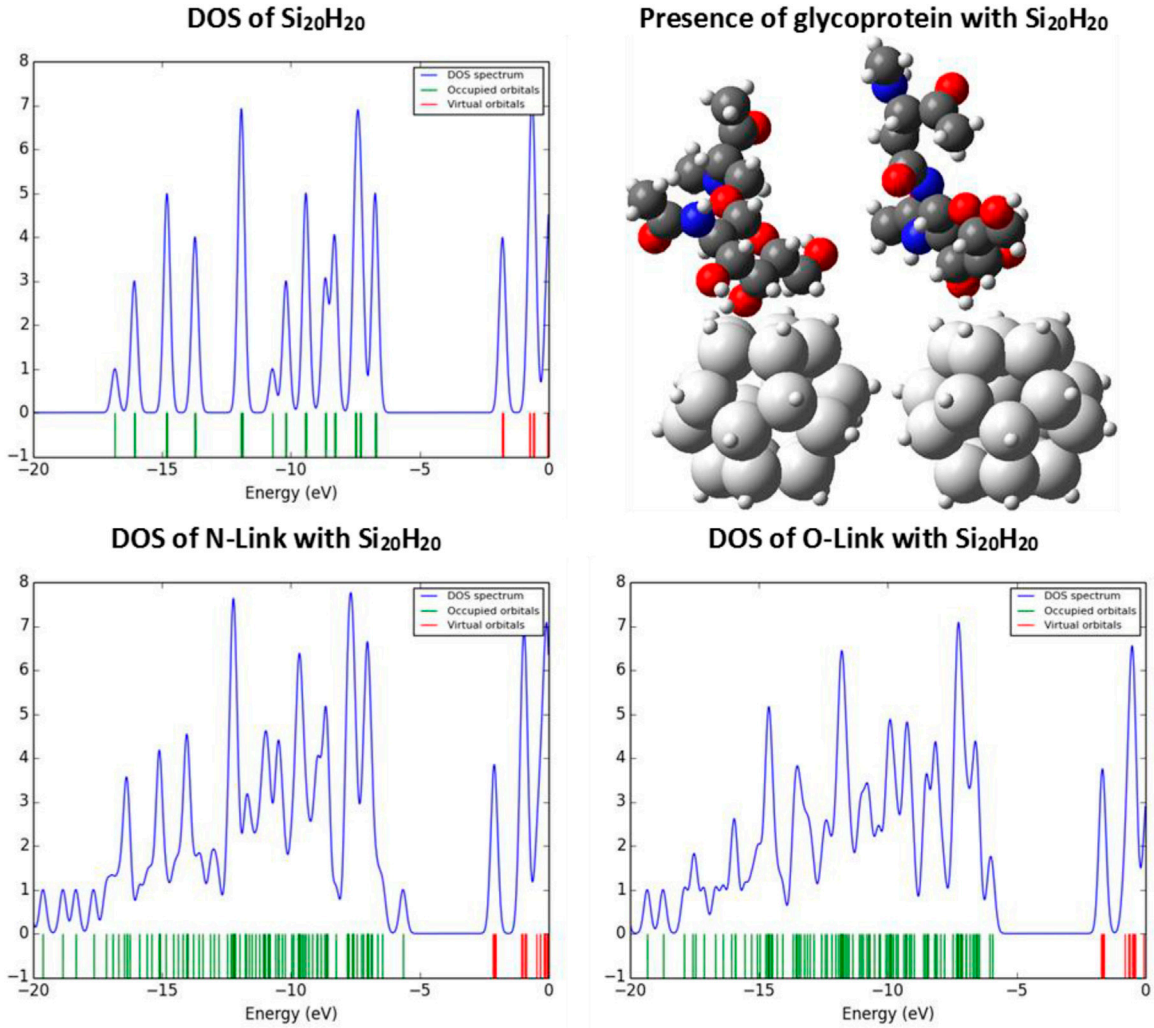

FIGURE 5 | The DOS diagrams of the $Si_{20}H_{20}$ in the absence and presence of N- and O-Link glycoproteins.

these two fullerenes will be similar. For this reason, comparing the values of the above specifications for the $Si_{20}H_{20}$ and $Si_{60}H_{60}$ structures, it cannot be concluded that these two structures have different electronic properties. Despite the different values of electrophilicity, even this sensitive index does not classify the two structures studied in different types. In the following, the structures of the studied sila-fulleranes are shown in **Figure 2**.

According to the data in **Table 1**. It can be concluded that the high chemical hardness combined with significant electron affinity of the sila-fulleranes, make them a good candidate for chemical sensors due to increased electronic interaction with the environment. To determine the advantage of fullerane structures over diamond structures, **Figure 3** shows the HOMO and LUMO orbitals in the smallest diamondoids, sila-diamondoids, and sila-fulleranes. The localized orbitals of HOMO and LUMO in diamonds and their silicon analogues mean that the electrons in their structure have less impact on the environment.

As mentioned earlier, we used the most symmetrical structures, to remove the effect of the edges. The formulas for our structures are $Si_{20}H_{20}$ and $Si_{60}H_{60}$, which have an icosahedral symmetry. The geometry of these two types of structures is shown in **Figure 4**.

Now, according to the data given in **Table 1**, our selected sample to save time in calculations, is the sila-dodecahedrane with the chemical formula $Si_{20}H_{20}$. We investigate the ability of the $Si_{20}H_{20}$ to see if it can sense the presence of the desired glycoproteins. We examine the reaction of $Si_{20}H_{20}$ to the presence of the desired glycoproteins with the probable changes in the density of states (DOS) diagram. **Figure 5** shows the changes in the diagram of the density of states of the $Si_{20}H_{20}$, due to the presence of N- and O-Link glycoproteins. The diagrams of this study are plotted with Gauss Sum software [50].

Silicon nanostructures have a very sensitive surface, so that in the face of high electronegative factors such as oxygen, its HOMO energy level increases, which is also confirmed by the density of states diagram, which it is confirmed by the density of states

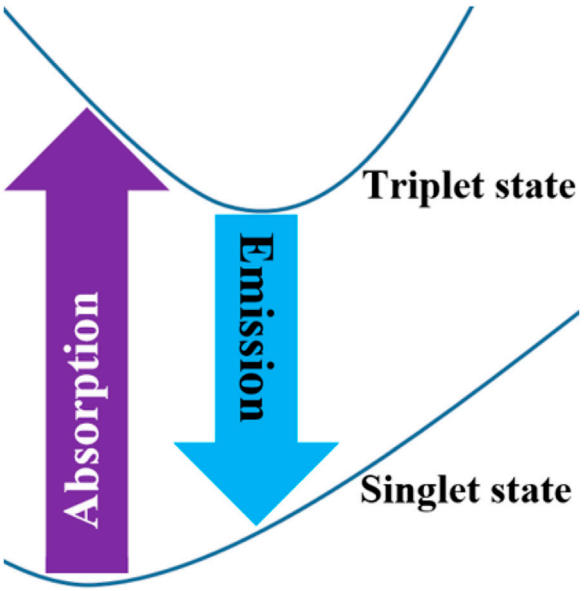

FIGURE 6 | The absorption and emission gaps of the system.

diagram. This is because the presence of oxygen increases the chemical potential of the structure and causes the electron to ionize or excite with less energy than before. So, changes in the DOS indicate differences in properties related to the electronic behaviors, such as optical properties. Now, we want to show how the color of the $Si_{20}H_{20}$ changes due to the presence of N- and O-Link glycoproteins?

Due to its large E_{Gap} of about 4.5 eV, the color of our nanoparticle should be white. In other words, since the spectrum of visible light, about 1.6–3.2 eV, does not have enough energy to act on the electrons of the $Si_{20}H_{20}$, the total radiation returned to space at each wavelength, without any absorption.

The calculation of the optical gap also confirms our results. Optical gaps are usually smaller than HOMO-LUMO gaps. The optical absorption gap can be calculated by subtracting the total energy of the optimized-ground state from the total energy of the excited state in the same ground state geometry, as shown in **Figure 6**.

Because the number of electrons of the $Si_{20}H_{20}$ is even, its spin state will be singlet, in the ground state. The lower-energy triplet excited-state is optically inactive, according to the $\Delta S = 0$ selection rule. Therefore, the lowest-energy allowed optical transition excites the system into the singlet excited state [51–55].

The energy of the singlet excited state is higher than the triplet state, due to larger repulsive Coulomb interactions between antiparallel spins. Therefore, the excited system may relax from the singlet state into the triplet one. Therefore, we calculate the emission bandgap from the relaxed excited triplet state to the ground state at the same energy, as shown in **Figure 6**. In **Table 2**, we present the calculated absorption and emission gaps of the $Si_{20}H_{20}$. The difference between the absorption and emission gaps shows the Stokes shift.

The calculated absorption and emission gaps confirm our prediction, that the color of the $Si_{20}H_{20}$ is white. Because the absorption gap is about 3.7 eV, and also, the emission gap is about 3.3 eV, none of them are in the range of the visible spectrum.

Our investigates show, the optimal distance between glycoprotein and sila-dodecahedrane depends on the condition and orientation of the glycoprotein relative to the sensor structure. But in general, it can be concluded that when the distance of hydrogens of both strucures have more than 2 Å of together, the energy of the correlation between them is close to zero. **Table 3** shows the electron properties of sila-dodecahedrane intracted to the studied glycoproteins.

Our calculations using AIM software analysis show that intermolecular interactions can take place between sila-dodecahedrane and glycoproteins in four zones (see **Figure 7**):

Zone (a): Between the hydroxyl oxygen of carbohydrate part of glycoprotein and the hydrogen sila-dodecahedrane, the distance between which is about 7.8 Å. At the critical point of this interaction, the electron density is about 0.0001 e.bohr^{-3} and the Laplacein density is about −0.0001 e.bohr^{-5}.

Zone (b): Between the carbonyl oxygen of carbohydrate part of glycoprotein and the hydrogen sila-dodecahedrane, the distance between which is about 2.2 Å. At the critical point of this

TABLE 2 | The absorption and emission gaps for the $Si_{20}H_{20}$ (in unit eV).

Spin state	Singlet (ground)	Triplet	Absorption gap	Singlet	Triplet (ground)	Emission Gap	Stoke shift
E_{Total}	−1,57,889.48	−1,57,885.77	3.71	−1,57,889.26	−1,57,885.94	3.32	0.39

TABLE 3 | A list of HOMO, LUMO and the H-L Gap for O and N-Link glycoproteins, $Si_{20}H_{20}$ and their complex systems together (in unit eV).

Structures	HOMO	LUMO	H-L gap
O-Link	−6.20	−0.98	5.22
N-Link	−6.13	−1.05	5.07
$Si_{20}H_{20}$	−6.83	−2.36	4.48
O-Link and $Si_{20}H_{20}$	−6.32	−2.07	4.25
N-Link and $Si_{20}H_{20}$	−6.06	−2.67	3.39

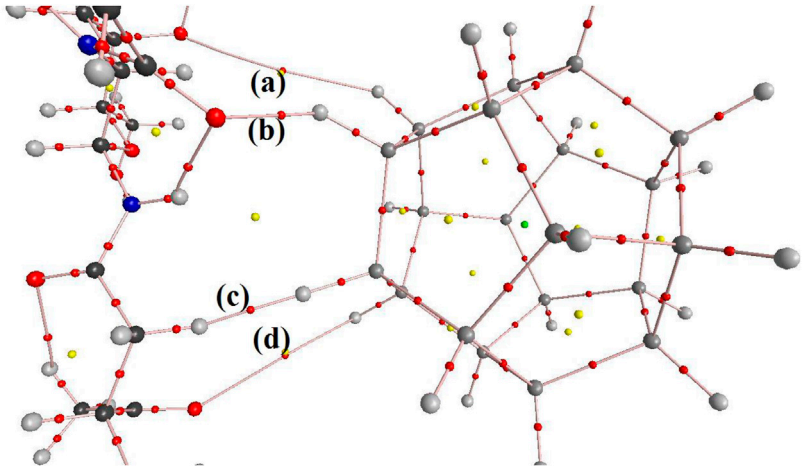

FIGURE 7 | AIM software analysis show that intermolecular interactions can take place between sila-dodecahedrane and glycoproteins in four zones.

interaction, the electron density is about 0.0179 e.bohr^{-3} and the Laplacein density is about −0.0147 e.bohr^{-5}.

Zone (c): Between the nearest hydrogens of glycoprotein and sila-dodecahedrane, the distance between which is about 2.0 Å. At the critical point of this interaction, the electron density is about 0.0112 e.bohr^{-3} and the Laplacein density is about −0.0080 e.bohr^{-5}.

Zone (d): Between the carbonyl oxygen of protein part of glycoprotein and the hydrogen sila-dodecahedrane, the distance between which is about 7.8 Å. At the critical point of this interaction, the electron density is about 0.0003 e.bohr^{-3} and the Laplacein density is about −0.0003 e.bohr^{-5}.

The following **Figure 8** shows the distance between atoms that interact with each other:

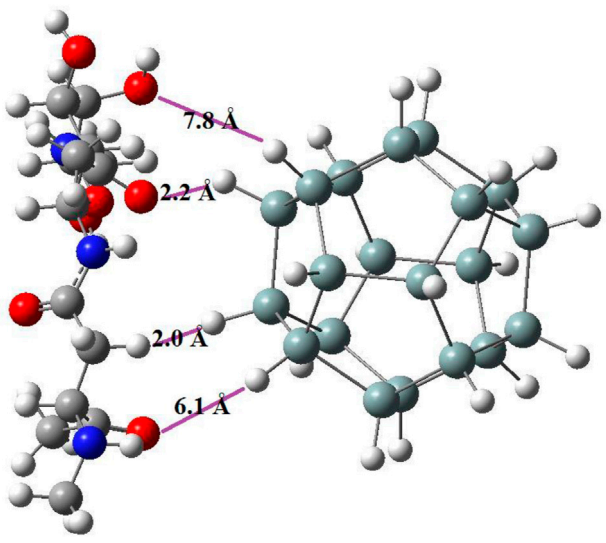

FIGURE 8 | The distance between the two structures of sila-dodecahedrane and glycoprotein in four zones that have intermolecular interaction.

Now, by obtaining the UV-Visible spectrum for the desired glycoproteins, we see that these structures also have no absorption in the visible spectrum [56]. The absorption range of N-Link and O-Link glycoproteins is in the ultraviolet part. But, interestingly, when van der Waals interaction between the $Si_{20}H_{20}$ and the desired glycoproteins is established, the absorption of the new combined system enters the visible region, as shown in **Figure 9**.

The details of our final absorption spectra for the complex system of sila-dodecahedrane and O and N-Linke glycoproteins are given below in **Table 4** using Gauss Sum software.

Since the absorption spectrum of the combined system of $Si_{20}H_{20}$ and desired glycoproteins also includes violet light, we expect to see the composite system in yellowish-green, based on the complementary wavelength [57–64].

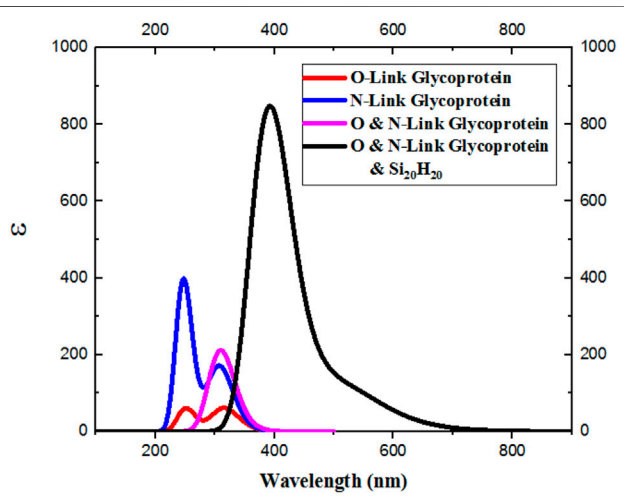

FIGURE 9 | Van der Waals interactions are established between the $Si_{20}H_{20}$ and N- and O-Link glycoproteins, the absorption in the new system also enters the visible spectrum.

TABLE 4 | The details of absorption spectra for the sila-dodecahedrane and O and N-Link glycoproteins.

Wavelength (nm)	Major contribs	Minor contribs
518.54	H-1→LUMO (21%), HOMO→LUMO (74%)	
432.10	H-1→LUMO (72%), HOMO→LUMO (21%)	HOMO→L+1 (4%)
405.45	HOMO→L+1 (88%)	H-2→LUMO (3%), H-1→LUMO (4%)
392.04	H-2→LUMO (78%)	H-9→LUMO (4%), H-6→LUMO (3%), H-3→LUMO
386.13	H-1→L+1 (92%)	HOMO→L+2 (2%)

Our investigations show that what is effective in changing the spectrum of optical absorption is the distance of oxygen of the protein part or the carbohydrate part of the glycoprotein from the surface of silicon nanoparticles. Because the presence of oxygen changes the electron density around the silicon nanoparticles, and it increases the dipole moment of the system from 0.002 about to 10 debye.

Since the electronic properties of silicon nanoparticles can be easily engineered, significant changes and desired color can be achieved by functionalizing the Si-nanoparticle surface. It should be noted that in 2015, Wagner et al. synthesized silicon dodecahedrane as a sila-fullerane with an endohedral chlorideIon [65].

CONCLUSION

The present study includes two crucial applications. First, the diagnosis of viral diseases by using diagnostic kits based on silicon nanoparticles, which are biocompatible, in addition to high electrical and optical sensitivity. Second, for environmental hygiene in the facades of houses, schools, etc. or urban structures, or at least handles or gloves, the coating of silicon nanoparticles can be used to detect viral contamination. Coronavirus (COVID-19) is an example of a viral infection that becomes a global problem today.

DATA AVAILABILITY STATEMENT

The raw data supporting the conclusions of this article will be made available by the authors, without undue reservation.

AUTHOR CONTRIBUTIONS

All authors listed have made a substantial, direct, and intellectual contribution to the work and approved it for publication.

ACKNOWLEDGMENTS

We gratefully acknowledge from Arshia Alaii, Mahdi Tavangar and Mohammad Parham Jafari for computational collaboration. The authors would also like to thank, Pedram and Parham Fathali Brothers, the young researchers of Rey1's Razi Pazhooheshsara's Nano Simulation Laboratory, because of their creative ideas.

REFERENCES

1. O'Neill MS. Helping Schoolchildren with Asthma Breathe Easier: Partnerships in Community-Based Environmental Health Education. *Environ Health Perspect* (1996) 104(5):464–6. doi:10.1289/ehp.96104464
2. Omar NAS, Fen YW, Abdullah J, Anas NAA, Ramdzan NSM, and Mahdi MA. Optical and Structural Properties of Cadmium Sulphide Quantum Dots Based Thin Films as Potential Sensing Material for Dengue Virus E-Protein. *Results Phys* (2018) 11:734–9. doi:10.1016/j.rinp.2018.10.032
3. Khalkhali M, Rostamizadeh K, Sadighian S, Khoeini F, Naghibi M, and Hamidi M. The Impact of Polymer Coatings on Magnetite Nanoparticles Performance as MRI Contrast Agents: a Comparative Study. *DARU J Pharm Sci* (2015) 23(1):1–12. doi:10.1186/s40199-015-0124-7
4. Hong SW, Kim DY, Lee JU, and Jo WH. Synthesis of Polymeric Temperature Sensor Based on Photophysical Property of Fullerene and Thermal Sensitivity of Poly(N-Isopropylacrylamide). *Macromolecules* (2009) 42(7):2756–61. doi:10.1021/ma802862h
5. Haino T, Araki H, Fujiwara Y, Tanimoto Y, and Fukazawa Y. Fullerene Sensors Based on Calix[5]arene. *Chem Commun* (2002)(18) 2148–9. doi:10.1039/b205048j
6. Cheng Z, Li Q, Li Z, Zhou Q, and Fang Y. Suspended Graphene Sensors with Improved Signal and Reduced Noise. *Nano Lett* (2010) 10(5):1864–8. doi:10.1021/nl100633g
7. Yavari F, and Koratkar N. Graphene-based Chemical Sensors. *J Phys Chem Lett* (2012) 3(13):1746–53. doi:10.1021/jz300358t
8. Robinson JT, Perkins FK, Snow ES, Wei Z, and Sheehan PE. Reduced Graphene Oxide Molecular Sensors. *Nano Lett* (2008) 8(10):3137–40. doi:10.1021/nl8013007
9. Romero JJ, Llansola-Portolés MJ, Dell'Arciprete ML, Rodríguez HB, Moore AL, and Gonzalez MC. Photoluminescent 1-2 Nm Sized Silicon Nanoparticles: A Surface-dependent System. *Chem Mater* (2013) 25(17):3488–98. doi:10.1021/cm401666a
10. Popplewell JF, King SJ, Day JP, Ackrill P, Fifield LK, Cresswell RG, et al.Kinetics of Uptake and Elimination of Silicic Acid by a Human Subject: a Novel Application of 32Si and Accelerator Mass Spectrometry. *J Inorg Biochem* (1998) 69(3):177–80. doi:10.1016/s0162-0134(97)10016-2
11. Park J-H, Gu L, Von Maltzahn G, Ruoslahti E, Bhatia SN, and Sailor MJ. Biodegradable Luminescent Porous Silicon Nanoparticles for *In Vivo* Applications. *Nat Mater* (2009) 8(4):331–6. doi:10.1038/nmat2398
12. Yu MK, Park J, and Jon S. Targeting Strategies for Multifunctional Nanoparticles in Cancer Imaging and Therapy. *Theranostics* (2012) 2(1):3–44. doi:10.7150/thno.3463
13. Connétable D, Timoshevskii V, Artacho E, and Blase X. Tailoring Band Gap and Hardness by Intercalation: An Ab Initio Study of I 8@ S I– 46 and Related Doped Clathrates. *Phys Re-view Lett* (2001) 87(20):206405. doi:10.1103/physrevlett.87.206405
14. Tournus F, Masenelli B, Mélinon P, Connétable D, Blase X, Flank AM, et al.Guest Displacement in Silicon Clathrates. *Phys Rev B* (2004) 69(3):035208. doi:10.1103/physrevb.69.035208
15. Kumar V, and Kawazoe Y. Hydrogenated Caged Clusters of Si, Ge, and Sn and Their Endohedral Doping with Atoms: Ab Initio Calculations. *Phys Rev B* (2007) 75(15):155425. doi:10.1103/physrevb.75.155425

16. Hao SG, Zhang DB, and Dumitrică T. Effect of Small Shape Changes on the Optical Response of Highly Symmetric Silicon Quantum Dots. *Phys Rev B* (2007) 76(8):081305. doi:10.1103/physrevb.76.081305
17. Fthenakis ZG, Havenith RW, Menon M, and Fowler PW. Structural and Electronic Properties of the Fullerene Isomers of Si 38: A Systematic Theoretical Study. *Phys Rev B* (2007) 75(15):155435. doi:10.1103/physrevb.75.155435
18. Zdetsis AD. One-nanometer Luminous Silicon Nanoparti-Cles: Possibility of a Fullerene Interpretation. *Phys Rev B* (2009) 79(19):195437. doi:10.1103/physrevb.79.195437
19. Kumar V, and Kawazoe Y. Hydrogenated Silicon Fullerenes: Effects of H on the Stability of Metal-Encapsulated Silicon Clusters. *Phys Rev Lett* (2003) 90(5):055502. doi:10.1103/physrevlett.90.055502
20. Zdetsis AD. Stabilization of Large Silicon Fullerenes and Re-lated Nanostructures through Puckering and Poly (Oligo) Merization. *Phys Rev B* (2009) 80(19):195417. doi:10.1103/physrevb.80.195417
21. Palagin D, and Reuter K. Evaluation of Endohedral Doping of Hydrogenated Si Fullerenes as a Route to Magnetic Si Building Blocks. *Phys Rev B* (2012) 86(4):045416. doi:10.1103/physrevb.86.045416
22. Marsusi F, and Qasemnazhand M. Sila-fulleranes: Promising Chemically Active Fullerene Analogs. *Nanotechnology* (2016) 27(27):275704. doi:10.1088/0957-4484/27/27/275704
23. Xie RH, Bryant GW, Zhao J, Kar T, and Smith VH, Jr. Tunable Optical Properties of Icosahedral, Dodecahedral, and Tetra-Hedral Clusters. *Phys Rev B* (2005) 71(12):125422. doi:10.1103/physrevb.71.125422
24. Karttunen AJ, Linnolahti M, and Pakkanen TA. Icosahedral Polysilane Nanostructures. *J Phys Chem C* (2007) 111(6):2545–7. doi:10.1021/jp067700w
25. Zdetsis AD. High-symmetry High-Stability Silicon Fuller-Enes: A First-Principles Study. *Phys Rev B* (2007) 76(7):075402. doi:10.1103/physrevb.76.075402
26. Sun Q, Wang Q, Briere TM, Kumar V, Kawazoe Y, and Jena P. First-principles Calculations of Metal Stabilized Si 20 Cages. *Phys Rev B* (2002) 65(23):235417. doi:10.1103/physrevb.65.235417
27. Palagin D, and Reuter K. MSi20H20 Aggregates: From Simple Building Blocks to Highly Magnetic Functionalized Materials. *ACS nano* (2013) 7(2):1763–8. doi:10.1021/nn3058888
28. Zhang IY, Wu J, and Xu X. Extending the Reliability and Applicability of B3LYP. *Chem Commun* (2010) 46(18):3057–70. doi:10.1039/c000677g
29. Lee C, Yang W, and Parr RG. Development of the Colle-Salvetti Correlation-Energy Formula into a Functional of the Electron Density. *Phys Rev B* (1988) 37(2):785–9. doi:10.1103/physrevb.37.785
30. Stephens PJ, Devlin FJ, Chabalowski CF, and Frisch MJ. Ab Initio calculation of Vibrational Absorption and Circular Dichroism Spectra Using Density Functional Force fields. *J Phys Chem* (1994) 98(45):11623–7. doi:10.1021/j100096a001
31. Cysewski P, Jeliński T, Przybyłek M, and Shyichuk A. Color Prediction from First Principle Quantum Chemistry Computations: a Case of Alizarin Dissolved in Methanol. *New J Chem* (2012) 36(9):1836–43. doi:10.1039/c2nj40327g
32. Castro A, Marques MAL, Alonso JA, and Rubio A. Optical Properties of Nanostructures from Time-dependent Density Functional Theory. *J Comput Theor Nanosci* (2004) 1(3):231–55. doi:10.1166/jctn.2004.2931
33. Tirado-Rives J, and Jorgensen WL. Performance of B3LYP Density Functional Methods for a Large Set of Organic Molecules. *J Chem Theor Comput.* (2008) 4(2):297–306. doi:10.1021/ct700248k
34. Hehre WJ, Ditchfield R, and Pople JA. Self-Consistent Molecular Orbital Methods. XII. Further Extensions of Gaussian-type Basis Sets for Use in Molecular Orbital Studies of Organic Molecules. *J Chem Phys* (1972) 56(5):2257–61. doi:10.1063/1.1677527
35. Ditchfield R, Hehre WJ, and Pople JA. Self-Consistent Molecular-Orbital Methods. IX. An Extended Gaussian-Type Basis for Molecular-Orbital Studies of Organic Molecules. *J Chem Phys* (1971) 54(2):724–8. doi:10.1063/1.1674902
36. Binkley JS, Whiteside R, Hariharan PC, Seeger R, Heh-re WJ, Lathan WA, et al.*GAUSSIAN 76: An Ab Initio Molecular Orbital Program (No. BNL-24136)*. Upton, NY (USA): Brookhaven National Lab. (1978). doi:10.2172/6738000
37. Petersson GA, Malick DK, Wilson WG, Ochterski JW, Montgomery JA, Jr, and Frisch MJ. Calibration and Comparison of the Gaussian-2, Complete Basis Set, and Density Functional Methods for Computational Thermochemistry. *J Chem Phys* (1998) 109(24):10570–9. doi:10.1063/1.477794
38. Bader RFW. *AIM2000 Program, v. 2.0*. Hamilton, Canada: McMaster University (2000)
39. Andersen KG, Rambaut A, Lipkin WI, Holmes EC, and Garry RF. The Proximal Origin of SARS-CoV-2. *Nat Med* (2020) 26(4):450–2. doi:10.1038/s41591-020-0820-9
40. Khalkhali M, Mohammadinejad S, Khoeini F, and Rostamizadeh K. Vesicle-like Structure of Lipid-Based Nanoparticles as Drug Delivery System Revealed by Molecular Dynamics Simulations. *Int J pharmaceutics* (2019) 559:173–81. doi:10.1016/j.ijpharm.2019.01.036
41. Watanabe Y, Berndsen ZT, Raghwani J, Seabright GE, Allen JD, Pybus OG, et al.Vulnerabilities in Coronavirus Glycan Shields Despite Extensive Glycosylation. *Nat Commun* (2020) 11(1):1–10. doi:10.1038/s41467-020-16567-0
42. Goutham S, Kumari I, Pally D, Singh A, Ghosh S, Akhter Y, et al.Mutually Exclusive Locales for N-Linked Gly-Cans and Disorder in Human Glycoproteins. *Scientific Rep* (2020) 10(1):1–12. doi:10.1038/s41598-020-61427-y
43. Amin M, Sorour MK, and Kasry A. Comparing the Binding Interactions in the Receptor Binding Domains of SARS-CoV-2 and SARS-CoV. *J Phys Chem Lett* (2020)
44. Qasemnazhand M, Khoeini F, and Marsusi F Fulleryne, a New Member of the Carbon Cages Family. arXiv preprint arXiv. 2020, 2003.09835.
45. Wang T, Lu J, Zhu H, Liu J, Lin X, Liu Y, et al.The Electronic Properties of Chiral Silicon Nanotubes. *Superlattices and Microstructures* (2017) 109:457–62. doi:10.1016/j.spmi.2017.05.034
46. Tavakol H, and Shahabi D. DFT, QTAIM, and NBO Study of Adsorption of Rare Gases into and on the Surface of Sulfur-Doped, Single-Wall Carbon Nanotubes. *J Phys Chem C* (2015) 119(12):6502–10. doi:10.1021/jp510508y
47. Zhan C-G, Nichols JA, and Dixon DA. Ionization Potential, Electron Affinity, Electronegativity, Hardness, and Electron Excitation Energy: Molecular Properties from Density Functional Theory Orbital Energies. *J Phys Chem A* (2003) 107(20):4184–95. doi:10.1021/jp0225774
48. Parr RG, Szentpály LV, and Liu S. Electrophilicity index. *J Am Chem Soc* (1999) 121(9):1922–4. doi:10.1021/ja983494x
49. Qasemnazhand M, Khoeini F, and Marsusi F. Predicting the New Carbon Nanocages, Fullerynes: A DFT Study. Scientific reports (2021) 11. doi:10.1038/s41598-021-82142-2
50. O'boyle NM, Tenderholt AL, and Langner KM. Cclib: A Library for Package-independent Computational Chemistry Algorithms. *J Comput Chem* (2008) 29(5):839–45. doi:10.1002/jcc.20823
51. Patrick CE, and Giustino F. Quantum Nuclear Dynamics in the Photophysics of Diamondoids. *Nat Commun* (2013) 4:2006. doi:10.1038/ncomms3006
52. Marsusi F, Sabbaghzadeh J, and Drummond ND. Compar-ison of Quantum Monte Carlo with Time-dependent and Static Densi-Ty-Functional Theory Calculations of Diamondoid Excitation Energies and Stokes Shifts. *Phys Rev B* (2011) 84(24):245315. doi:10.1103/physrevb.84.245315
53. Shu Y, Fales BS, and Levine BG. Defect-induced Conical Intersections Promote Nonradiative Recombination. *Nano Lett* (2015) 15(9):6247–53. doi:10.1021/acs.nanolett.5b02848
54. Marsusi F. Nuclear Dynamic Effects on Electronic Properties of Functionalized Diamondoids. *Physica E: Low-dimensional Syst Nanostructures* (2018) 103:435–43. doi:10.1016/j.physe.2018.05.010
55. Qasemnazhand M, Khoeini F, and Shekarforoush S. Electronic Transport Properties in the Stable Phase of a cumulene/B7/cumulene Molecular Bridge Investigated Using Density Functional Theory and a Tight-Binding Method. *New J Chem* (2019) 43(42):16515–23. doi:10.1039/c9nj02860a
56. Alrikabi A. Theoretical Study of the Design Dye-Sensitivity for Usage in the Solar Cell Device. *Results Phys* (2017) 7:4359–63. doi:10.1016/j.rinp.2017.07.022
57. Pickering C, Beale MIJ, Robbins DJ, Pearson PJ, and Greef R. Optical Studies of the Structure of Porous Silicon Films Formed in P-type Degenerate and Non-degenerate Silicon. *J Phys C: Solid State Phys* (1984) 17(35):6535–52. doi:10.1088/0022-3719/17/35/020
58. Canham LT. Silicon Quantum Wire Array Fabrication by Electrochemical and Chemical Dissolution of Wafers. *Appl Phys Lett* (1990) 57(10):1046–8. doi:10.1063/1.103561

59. Belomoin G, Therrien J, Smith A, Rao S, Twesten R, Chaieb S, et al.Observation of a Magic Discrete Family of Ultrabright Si Nanoparticles. *Appl Phys Lett* (2002) 80(5):841–3. doi:10.1063/1.1435802
60. Kanemitsu Y. Light Emission from Porous Silicon and Related Materials. *Phys Rep* (1995) 263(1):1–91. doi:10.1016/0370-1573(95)00021-4
61. Veinot JGC. Synthesis, Surface Functionalization, and Properties of Freestanding Silicon Nanocrystals. *Chem Commun* (2006)(40) 4160–8. doi:10.1039/b607476f
62. Yang L, Liu Y, Zhong Y-L, Jiang X-X, Song B, Ji X-Y, et al.Fluorescent Silicon Nanoparticles Utilized as Stable Color Converters for white Light-Emitting Diodes. *Appl Phys Lett* (2015) 106(17):173109. doi:10.1063/1.4919526
63. Fu YH, Kuznetsov AI, Miroshnichenko AE, Yu YF, and Luk'yanchuk B. Directional Visible Light Scattering by Silicon Nanoparticles. *Nat Commun* (2013) 4(1):1–6. doi:10.1038/ncomms2538
64. Harun K, Salleh NA, Deghfel B, Yaakob MK, and Mohamad AA. DFT + U Calculations for Electronic, Structural, and Optical Properties of ZnO Wurtzite Structure: A Review. *Results Phys* (2020) 16:102829. doi:10.1016/j.rinp.2019.102829
65. Tillmann J, Wender JH, Bahr U, Bolte M, Lerner H-W, Holthausen MC, et al.One-Step Synthesis of a [20]Silafullerane with an Endohedral Chloride Ion. *Angew Chem Int Ed* (2015) 54(18):5429–33. doi:10.1002/anie.201412050

Conflict of Interest: The authors declare that the research was conducted in the absence of any commercial or financial relationships that could be construed as a potential conflict of interest.

Copyright © 2021 Qasemnazhand, Khoeini and Marsusi. This is an open-access article distributed under the terms of the Creative Commons Attribution License (CC BY). The use, distribution or reproduction in other forums is permitted, provided the original author(s) and the copyright owner(s) are credited and that the original publication in this journal is cited, in accordance with accepted academic practice. No use, distribution or reproduction is permitted which does not comply with these terms.